International Journal of Science and Research (IJSR)
ISSN: 2319-7064
SJIF (2022): 7.942

Influence of Tin Contamination on the Posse Gap and Added Constraints of Unstructured Se-Te Tinny Films

Vinyas Goswami[1], Satendra Singh[2]

[1]Research Scholar, Department of Physics, Sunrise University, Alwar, Rajasthan, India

[2]Associate Professor, Department of Physics, Sunrise University, Alwar, Rajasthan, India

Abstract: ***Thin strips of the unmolded Se40-xTe60Snx glassy mixture were measured under high vacuum conditions (10-5 Torr) in the range 200-3000 nm with a computer-controlled double-beam UV-VIS-NIR spectrophotometer. Synthesized by thermal evaporation mode. Optical constants (refractive index (n), real permittivity (ε'), imaginary permittivity (ε''), and immersion measurements (α)) of unshaped Se40-xTe60Snx thin films using the Swanepolemode) and the optical bandgap were calculated. strip. The immersion level (α) increases with incident photon energy (hν) for all samples. The optical bandgap increases with increasing drum content (Sn).***

Keywords: Chalcogenide spectacles, Thin film, optic constants, optic band gap etc.

1. Introduction

Thin strips of unshaped chalcogenides have attracted much attention due to their interesting electrical, optical and thermal packages (1-3) with new advanced and interchangeable technological materials. The long refractive indicator range and low optical loss enable their development as infrared optics (4). The lack of long-range order in these glasses allows the optical package to be reworked and the composition to be changed continuously for specific technological operations. The study of the optical constants of endowments is attractive because these endowments are used in optical filaments and the optical package of all endowments is related to their microstructure, electronic and band structure. One of chalcogenide glass Se40-xTe60Snx thin films. Glassy Se-Te amalgamation has important implications among chalcogenide glasses. This is because compared to pure Se, it has higher photosensitivity, lower hardness, higher crystallization temperature, lower aging effect (5), and is useful for practical operations (6). Since each contamination sliver meets its needs by adapting to the adjacent terrain, contamination was thought to have little effect on unformed semiconductor packages. Part of a colorful essence similar to Ag, Snetc. Considerable attention has been paid to the 'additions' affecting chalcogenide eyeglass packages (7, 8). It is fascinating to study the contribution of Ag, Sn essences to influence the spectacle package of Se-Te system. In this communication, we report the effects of Sn and Ag chips on the optical packets of Se-Te systems. Sn is chosen as a cumulative ingredient because it mixes with the highest essences and modifies the physical package. Knowing the exact value of the wavelength-dependent refractive index of a thin strip of light provides alphanumeric information about the optical energy gap (eg), the strain regime, phonon and tube abundances, and more. A material's optical gesture determines its optical constants. Optical constants such as refractive index (n) and annihilation (k) are determined by the well-known Swanepoel system (9), Use a transmission diapason in the UV-VIS-NIR range. Immersion measurement analysis was also performed to determine the Eg and nature of the transition. In fact, since the late 1960s, it has become common to modify the packaging of chalcogenide goggles by adding various elements. Sn-containing chalcogenide eyeglasses have attracted considerable interest in glass wisdom and technology, with Abecedarian studies on their structure, packaging, and pharmacotherapy (10-14). They are present in numerous current fields in optics, optoelectronics, chemistry and biology, as well as in optical fundamentals, gratings, photodoping, optical memories, micro-lenses, surge companions, holography, memoir and chemical detectors, solid electrolytes, batteries, etc. has an operation of (15-24). The effect of contamination on unformed semiconductor materials is highly dependent on the conducting medium and material structure (25). Contamination can destroy pendant binding centers of labels or form charged centers that are compensated by centers of opposite sign. In this study, Sn was chosen as the cumulative element in the Se–Te mixture. The third element is reported to extend the range of glass formation and thus acts as a chemical modifier. The addition of a third element such as Sn in Se-Te double fusion is expected to modify the optical and electrical package of the host fusion. Typical chalcogenides have fairly sharp optical immersion edges, a single electrical activation energy, effective conductivity, and fluorescence upon compressive motion. Studying the optical package of chalcogenide glasses is important for determining the electronic band structure and other optical parameters as well as the optical energy gap and refractive index. At the end of this work, we investigate the effect of her Sn objectification on the optical packets of Se–Te mixtures. The optical transmittance scale of unshaped a-Se40-xTe60Snx thin films is measured with a spectrophotometer.

Procedure of Experiment

Glassy mixtures of a-Se40-xTe60Snx (x = 0, 2, 4, 6, 8) were prepared by melt quenching. Accurate proportions of highly pure 99.999 Se0, Sn and Te particles were loaded according to the equation a-Se40-xTe60Snx (x = 0, 2, 4, 6, 8). The fat color mixture was placed in a quartz vial and sealed under a vacuum of 10-5 Torr. The sealed quartz ampoule was loaded

into a furnace, heated to 950 °C for 18 h at a rate of 3–4 C/nsec to ensure compositional homogeneity, and quenched with liquid nitrogen. The beams were squashed, separated, predicted and characterized. The glassy nature of the mixture was confirmed by X-ray diffraction patterns using Cu-Kα radiation. Chalcogenide flakes were synthesized by thermal evaporation under high vacuum conditions (10-5 Torr) using bulk fusion flakes as starting materials and glass as substrate. The strip was kept in the deposition chamber for 24 hours to achieve metastable equilibrium. Optical transmittance scales of thin strips of unmolded Se40-xTe60Snx (x = 0, 2, 4, 6, 8) were measured at wavelengths using a computer-controlled dual-beam UV-VIS-IR spectrophotometer measured as a function.

2. Results and discussion

The optical system considered is unformed, homogeneous, and unchanging. Swanepole's known system, based on Mainfacer's proposition (26), causes envelopes of disturbance maxima and minima to occur in the film, and the presence of these maxima and minima positions gives rise to optical unification of the deposited film. confirmed, Nr scattering and immersion occur at: long wavelength. This mode was used by colorful experimenters with chalcogenide glasses (27–28).

In Swanepole's system, the optical parameters are derived from the boundary pattern of the transmission diapason. In the transmission range where the immersion is (α = 0), the refractive index n is given by

$$n = [N+ (N2-s2)^{1/2}]^{1/2} \quad (i)$$

where N = (2s Tm)-(s2 1) / 2, s is the refractive index of the substrate, and Tm is the transmission minimum envelope function.

where (α ≠ 0), in the low and medium immersion range, the index of refraction n is given by

$$N = [N+ (N2-s2)^{1/2}]^{1/2} \quad (ii)$$

where N = { 2s (TM-Tm) / TMTm (s2 1) / 2 and Tm is the envelope function of the transmission maximum.

In regions of deep immersion, the transmittance drops significantly and the refractive index (n) can be estimated considering the values in other regions. If n1 and n2 are the indices of refraction at two adjacent maxima and minima of λ1 and λ2, then the film consistency (d) is also given by

$$d = \lambda1\lambda2/ 2 (\lambda1n2-\lambda2n1) \quad (iii)$$

The extermination measure (k) can be calculated by relation

$$k = \alpha \lambda/ (4\pi) \quad (iv)$$
$$= (\lambda/ 4\pi d) \ln (1/ x)$$

where x is the absorbance and d is the film density. For weak and medium immersion regions, the absorbance (x) can be calculated from the transmission minimum Tm and is given by:

$$x = (Em-\{ Em-(n2-1) 3 (n2-s4) 1/2) / ((n-1) 3 (n-s2)) \quad (v)$$

where Em = ((8n2s Tm)-(n2-1) (n2-s2))

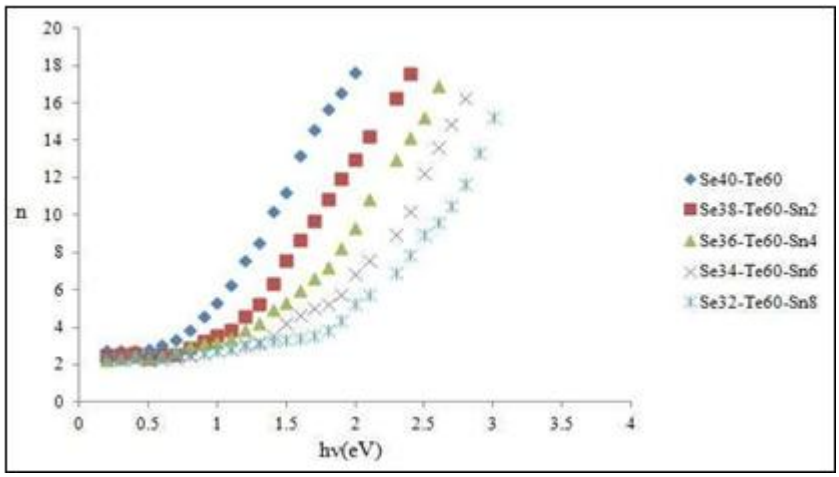

Figure 1: Variation of refractive index (n) with photon energy (hv) for amorphous $Se_{40-x}Te_{60}Sn_x$ thin film

The values obtained for the refractive index and the degree of breakdown are shown in Table 1. Figure 1 shows the change in refractive index with photon energy (hv), and Figure 1 shows the change in annihilation scale with photon energy.2. Refractive index values and annihilation measurements have been observed to show an overall increasing trend with increasing photon energy. From Table 1, it can be seen that the values of refractive index (n) and breaking strength (k) increase with increasing Sn content in a-Se40-xTe60Snx thin films. This spectral and doping dependence of optical constants on photon energy helps determine whether this system is suitable for optical data storage bias operations. The real and imaginary corridors of permittivity of undeformed thin strips were calculated independently of the relationship

$$\varepsilon' = n2 – k2 \quad (vi)$$
$$\varepsilon'' = 2nk \quad (vii)$$

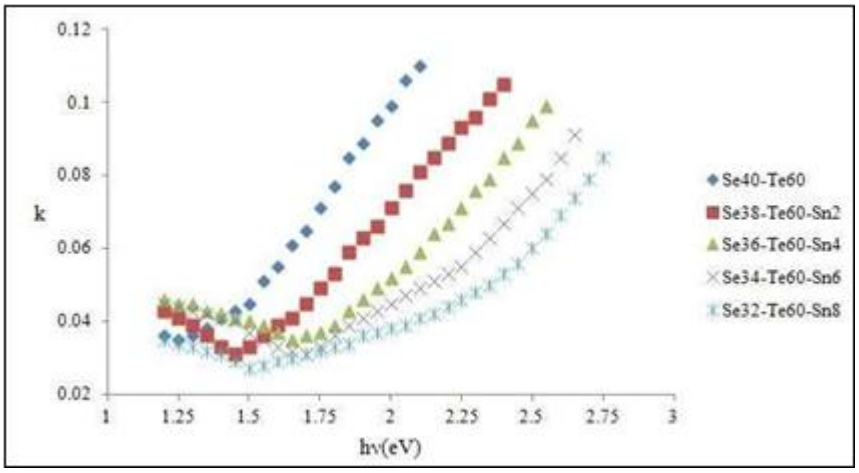

Figure 2: Variation of extinction Coefficient (k) with photon energy (hv) for amorphous $Se_{40-x}Te_{60}Sn_x$ thin film

Material	Refractive Index (n)	Extinction Coefficient (k)	Real Dielectric Constant (ε')
Se40Te60	17.66	0.099	133.00
Se38Te60Sn2	12.95	0.071	65.00
Se36Te60Sn4	9.35	0.052	50.00
Se34Te60Sn6	6.85	0.045	34.00
Se32Te60Sn8	5.25	0.038	19.00

Table1: Optical constants for amorphous Se TeSn thin films at 1600nm.

Imaginary Dielectric Constant (ε')	Absorption O Coefficient (α) (m^{-1}) x10	Optical t Band[3] GapEg (e V)
2.45	28.00	.78
1.55	16.00	1.13
0.79	10.00	1.25
0.53	6.66	1.33
0.35	4.10	1.42

Corridors of the real and imaginary permittivity with photon energy are shown in Figures 1 and 2.3 and 4 are independent. The calculated real and imaginary parts of the permittivity are also shown in Table 1. These are set to increase with increasing photon energy and with the addition of Sn contamination to the current a-Se40-xTe60Snx thin-strip system.

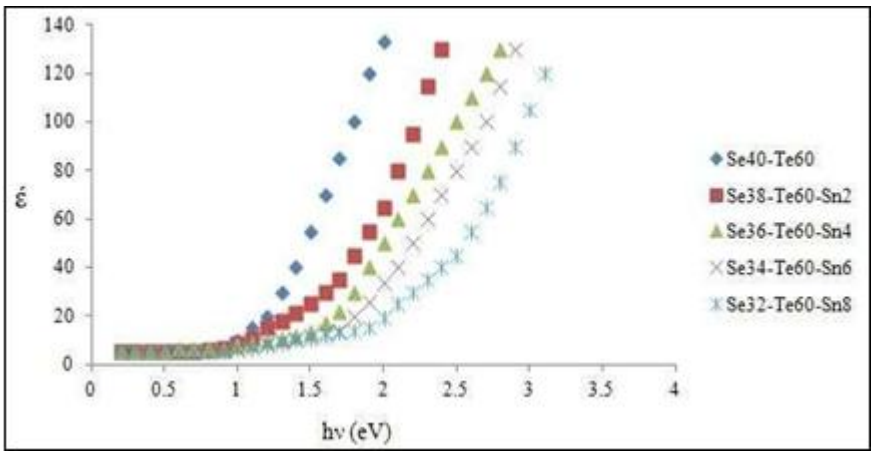

Figure 3: Variation of real dielectric constant (ε') with photon energy (hv) for amorphous $Se_{40-x}Te_{60}Sn_x$ thin film

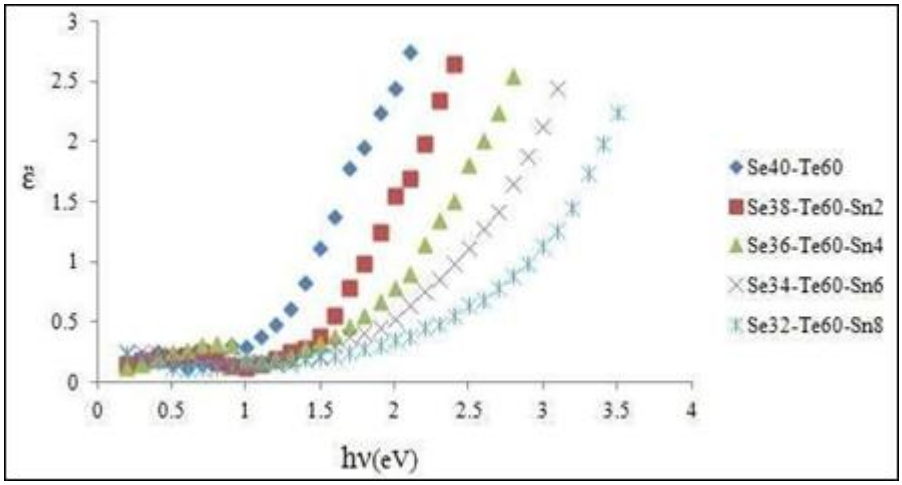

Figure 4: Variation of imaginary dielectric constant with photon energy (hv) for amorphous $Se_{40-x}Te_{60}Sn_x$ thin film

Immersion Measure and Optical Band Gap

The immersion measure (α) of unformed Se40-xTe60Snx thin flicks have been Calculated by using relation (viii)

$$\alpha = 4\pi k/\lambda \quad \text{(viii)}$$

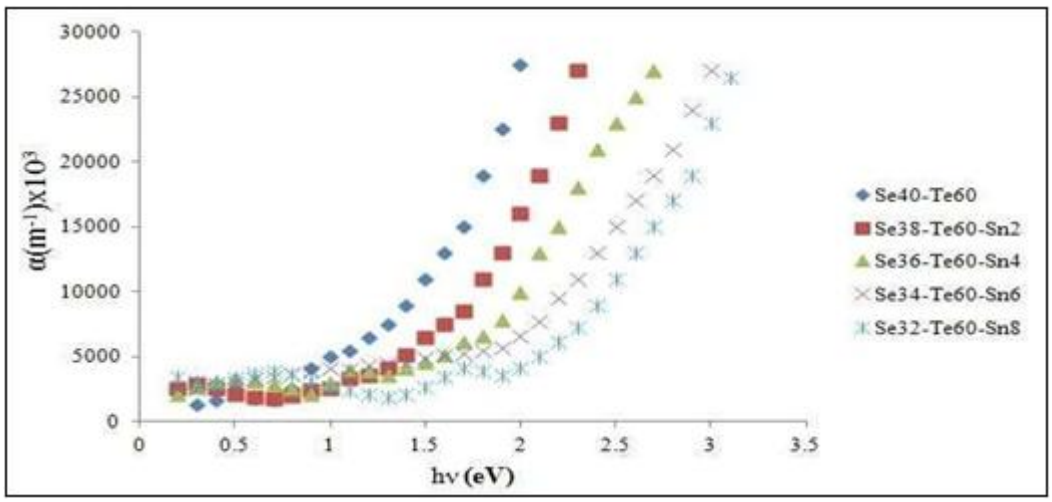

Figure 5: Variation of absorption coefficient (α) with photon energy (hv) for amorphous $Se_{40-x}Te_{60}Sn_x$ thin film

Secondly, it is also observed that the value of immersion (α) increases with increasing photon energy in a-Se40-xTe60Snx flakes, and that the value of immersion increases with increasing Sn content. Due to their high immersion, these configurations may be suitable for optical memory biasing. The optical bandgap is calculated from the immersion measurement data as a function of energy (hv) using the Tauc relation (30). α = A (hn-Eg) n/ hn (ix) where A is a constant, Eg is the optical bandgap of the material, and the exponent n depends on the type of transition, with values of 1/2 and 2.3. /2 and 3 independently of each other correspond to allowed direct, allowed cyclic, forbidden direct, and forbidden cyclic transitions.

The current system of a-Se40-xTe60Snx follows the allowed circular transition rule. Optical bandgap (Eg) values are calculated by establishing the linear segment of (αhv) 1/nvs. Calculate hv for n = 2 as shown.6. Calculated values of Eg for all samples are shown in Table 1. From Table 1, it can be seen that the optical bandgap (Eg) increases as the Sn content increases. The increase in optical bandgap with increasing Sn content can be explained based on the model by Mott and Davis (29). According to this epidemic, strain states are of great interest in chalcogenide thin films, and these corruptions are responsible for the presence of localized states within the bandgap. The increase in the optical bandgap with increasing Sn content could be due to a decrease in viscosity or an increase in disorder in the strain lands of the mobility gap. The increase in optical bandgap with decreasing viscosity of the deformed land can also be discerned by the electronegativities of the primordial groups involved. The electronegativities of Se, Te, and Sn are 2.4, 2.1, and 1.96, respectively, with Sn being more electronegative than Se. The flounce bands of the chalcogenide glasses contain the p-orbitals of the credit bracket, and the addition of the electropositive element (Sn) to the electronegative element (Se) increases the energy of the credit bracket country and the credit bracket range expands further. It flounces the band within the forbidden bandgap, leading to band trailing and widening of the bandgap.]

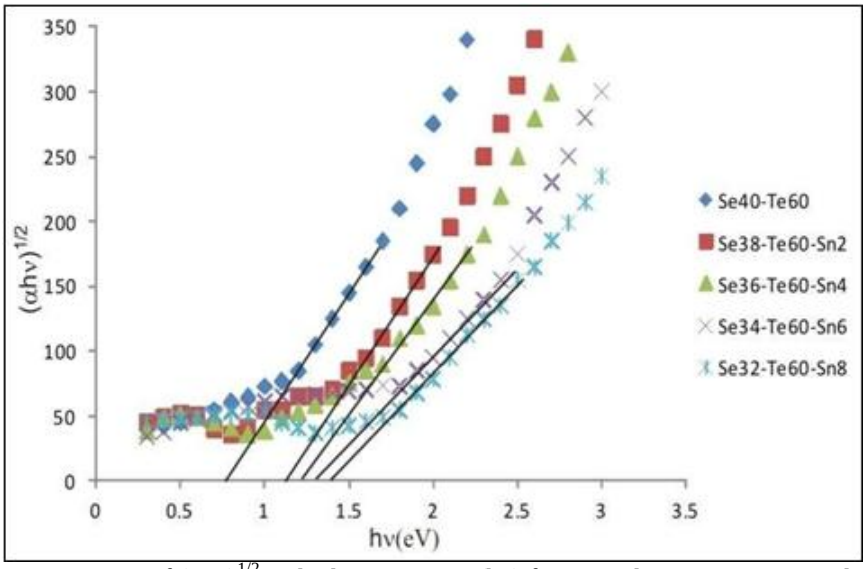

Figure 6: Variation of $(\alpha h\nu)^{1/2}$ with photon energy (hv) for amorphous $Se_{40-x}Te_{60}Sn_x$ thin film

These circular bandgap instruments can operate implicitly in optical recording media, infrared spectroscopy, filament emission, xerography, fiber optic communications, and electrophotographic manipulation. Refractive index and translucency in the infrared are also good indicators for integrated optics and discoveries in the near-infrared spectral range.

3. Conclusion

The optical gap increases with increasing Sn attention in the Se40-xTe60Snx system (x = 0, 2, 4, 6, and 8). The results prove that the optical gap is explosively dependent on the film composition. The degree of film immersion directly depends on the photon energy. Over a wide wavelength range, the immersion volume follows the Urbach relation (31). We also found that the values of the optical constants increased with the addition of Sn content at room temperature. The increase in optical bandgap with the addition of Sn content can be attributed to the increase in grain size, decrease in complaint and decrease in viscosity in the blemish state, leading to less smear of ribbon.

References

[1] H. B. Chung, K. Shin, Jae-MinLee, J. Vac. Sci. Technol. A25, (2006) 48.
[2] M. S. Kamboj, G. Kaur, R. Thangaraj, D. K. Avasthi, J. Phys. D: Appl Phys.35, (2002) 477.
[3] Uddin, H. Howari, andG. A. Ansari Chalcogenide letters Vol. 13 (March 2016) pp.117-125
[4] E. R. Shaaban, M. A. Kaid, E. L. Sayed Moustfa, A. Adel, J. Phy. D: Appl. Phy.41, (2008) 125307.
[5] S. O. Kasap, T. Wagner, V. Aiyah, O. Krylouk, Berkirov, L. TichyJ. Mater. Sci.34, (1999) 3779.
[6] J. S. Sanghera, L. B. Shaw, I. D. Aggarwal, Comptes Rendus Chimie 5, (2002) 873.
[7] N. Mehta, D. Sharma, A. Kumar, PhysicaB391, (2007) 108.
[8] R. S. Kundu, K. L. Bhatia, Nawal Kishore, V. K. Jain, PhysicaB74, (1996) 317.
[9] R. Swanepoel, J. Phys. E: Sci. Instrum.16, (1983) 1214.
[10] D. P. Gosain, T. Shimizu, M. Ohmuru, M. Suzuki, T. Bando, S. Okano, J. Mat. Sci.26, (1991) 3271.
[11] K. Uchino, K. Takada, T. Ohno, H. Yoshida, Y. Kobayashi, Jpn. J. Appl. Phys.31, (1993) 5354.
[12] N. Nobukuni, M. Takashima, T. Ohno, M. Ohrie, J. Appl. Phys.78, (1995) 6980.
[13] M. Nakamura, Y. Wang, O. Matsuda, K. Inoue, K. Murase, J. Non-cryst. Solids740, (1996) 198-200.
[14] L. Men, F. Jiang, F. Gan, Mater Sci. Eng. B18, (1997) 47.
[15] R. V. Woudenberg, Jpn. J. Appl. Phys.37, (1998) 2159.
[16] T. Z. Babeva, D. Dimitrov, S. Kitova, I. Konstantinov, Vacuum 58, (2000) 96.
[17] V. Mikla, I. P. Mikhalko, V. V. Mikla, MaterSci. Eng. B83, (2001) 74.
[18] K. Kolobov, J. Tominaga, J. Optoelectron. Adv. Mater4 (3), (2002) 679.
[19] S. A. Khan, M. Zulfequar, M. Hussain, Vacuum72, (2003) 291.
[20] K. Tanaka, J. Non-cryst. Solids1179, (1993) 164.
[21] T. Kawaguchi, S. Maruno, S. R. Elliot, J. Appl. Phys.79, (1996) 9096.
[22] M. Ohto, PhysStatus Solidi A 159, (1997) 461.
[23] Kumar, P. B. Barman, R. Sharma, Adv. Appl. Sci. Research1 (2), (2010) 47.
[24] Kumar, M. Lal, K. Sharma, S. K. Tripathi, N. Goyal, Chalc. Lett.9, (2012) 275.
[25] ArpitKaistha, V. S. Rangraand Pankaj Sharma, Chalc. GlassVol.41, No.2, (2015) 175-179
[26] J. C. Manifacier, J. Gasiot, J. P. Fillard, J. Phys. E. Sci. Instrum.9, (1976) 1002.
[27] S. M. Ei-Sayed, Vaccum72, (2004) 169.
[28] H. S. Metcoally, Vaccum62, (2001) 345.
[29] N. F. Mott, E. A. Davis, Electronic Processes in Non-CrystallineMat., Clarendon, Oxford, (1979) 428.
[30] M. M. Wakkad, E. Kh. Shoker, S. H. Mohamed, J. Non-Cryst. Solids157, (2000) 265.
[31] Urbach Source: Physics Review, 13 (1953) 92